# **ORGANOMETALLICS**

pubs.acs.org/Organometallics Article

# Multisite Ligand Noninnocence of (Cp<sup>N3</sup>)Fe(CO)<sub>3</sub><sup>+</sup> with Exogenous Hydride Donors: Kinetics and Mechanism

Andrew I. VanderWeide, Hagen Neugebauer, Bhumika Goel, David S. Tresp, Deuris Pena, Stefan Grimme, Andreas Hansen, and Demyan E. Prokopchuk\*



Cite This: https://doi.org/10.1021/acs.organomet.4c00137



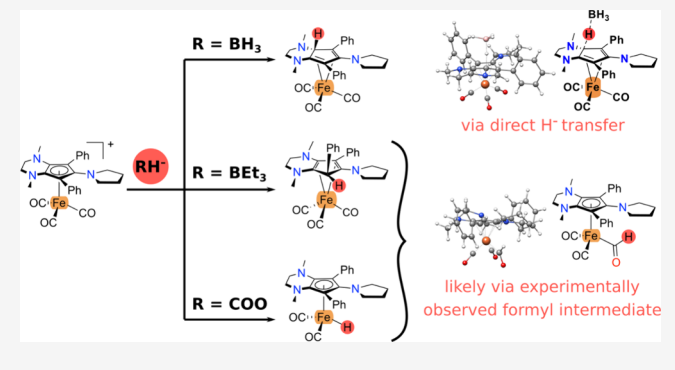
**ACCESS** I

III Metrics & More

Article Recommendations

SI Supporting Information

**ABSTRACT:** We show that amine-rich  $Cp^{N3}$  ligands coordinated to iron display chemically noninnocent behavior in the presence of exogenous hydride donors  $(Cp^{N3} = 1,4\text{-dimethyl-5,7-diphenyl-6-(pyrrolidin-1-yl)-2,3,4,6-tetrahydro-1<math>H$ -cyclopenta[b]pyrazin-6-yl). The reaction of piano-stool iron complex  $[(Cp^{N3})Fe(CO)_3]^+$  with three different hydride reagents furnishes three different iron complexes, two of which result in net  $H^-$  transfer to the  $Cp^{N3}$  ligand. Exposure of  $[(Cp^{N3})Fe(CO)_3]^+$  to NaHBEt $_3$  results in endo hydride addition to the  $Cp^{N3}$  ligand, reaction with NaBH $_4$  yields an exo- $Cp^{N3}H$  product, and an iron hydride complex forms in the presence of  $[^nBu_4N][HCOO]$ . While state-of-the-art DFT computations indicate that NaBH $_4$  addition to  $[(Cp^{N3})Fe(CO)_3]^+$  happens via direct  $H^-$  transfer to the  $Cp^{N3}$  ligand, reactions with



HBEt<sub>3</sub><sup>-</sup> or HCOO<sup>-</sup> initially generate a key iron formyl intermediate which has been experimentally observed. Herein, we present a blend of experimental and computational data to unravel some elementary steps that lead to the formation of these chemically distinct hydride addition products.

### INTRODUCTION

Cyclopentadienyl (Cp) ligands are privileged in organometallic chemistry and most often operate as ancillary ligands, retaining their maximum hapticity ( $\eta^5$ -Cp) when coordinated to transition metals. 1-5 However, coordinatively saturated metal complexes bearing  $\eta^5$ -Cp have been shown to react with nucleophiles, electrophiles, or radicals, undergoing an  $\eta^5$  to  $\eta^4$ hapticity change.<sup>6</sup> Nucleophilic addition reactions to metallocenes  $[Cp_2M]^+$  (M = Co, Rh) were pioneered by Wilkinson by using lithium aluminum hydride to give  $(\eta^4$ -CpH)MCp complexes (A; R = H, Scheme 1). Additionally,  $(\eta^4$ - $C_5H_4RH)CoCp$  complexes (A; R = Alkyl, Ph, PhO<sup>-</sup>) were accessed by addition of nucleophiles to cobaltocenium salts.<sup>8-10</sup> These exo addition products have been rationalized within the context of the Davies-Green-Mingos rules for nucleophilic addition to hydrocarbon ligands (i.e., preferential nucleophilic attack on the exo face of coordinated polyene rings).<sup>11</sup> Reactivity was also expanded to include the pianostool complex CpFe(CO)<sub>2</sub>(PPh<sub>3</sub>) (B) via reaction with NaBH<sub>4</sub>. The synthesis of B was later revisited by Astruc, who found that the iron formyl intermediate CpFe(CO)-(CHO)(PPh<sub>3</sub>) is generated prior to Cp ring activation, suggesting that endo ring activation might be operative; however, no further mechanistic work was carried out to delineate between endo and exo ring addition.<sup>13</sup>

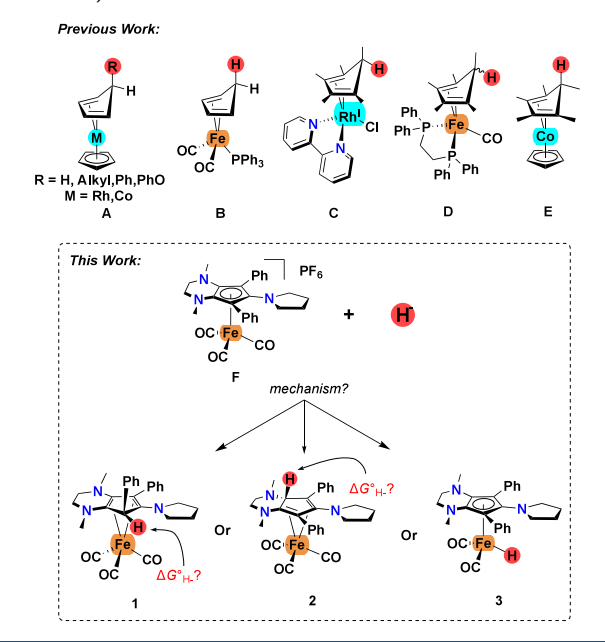
The movement of hydride  $(H^{-})$ , the simplest nucleophile, is of major importance in chemical energy conversion processes, <sup>14</sup> and it has recently been shown that  $(\eta^4$ -CpH)M complexes bearing an C(sp<sup>3</sup>)-H bond in the diene ring can act as hydride transfer agents to small molecules. The endo-Cp\*H complex  $(\eta^4-C_5Me_5H)RhCl(bpy)$  (C) has an aqueous hydricity ( $\Delta G_{\rm H-}$ ) of 23 kcal/mol and performs hydride transfer to the enzyme cofactor NAD<sup>+</sup> ( $\Delta G_{H-}$ (NADH) = 28 kcal/mol). The complex  $(\eta^4-C_5Me_5H)Fe(dppe)(CO)$  (D) can be synthesized as the endo- or exo-Cp\*H adduct with exo formation occurring via addition of LiHBEt, to [(Cp\*Fe- $(dppe)(CO)^{+16,17}$  endo-D and the exo complex  $(\eta^4$  $C_5Me_5H)CoCp^*$  (E) are capable of transferring H<sup>-</sup> to  $CO_2$ to generate formate (HCOO<sup>-</sup>) in acetonitrile. 17,18 Notably, the endo hydrogens in complexes C and endo-D are generated through intramolecular metal-to-ligand migration via Rh-H and Fe-H intermediates and not via nucleophilic attack using exogenous hydride donors.

Special Issue: Experimental Studies of Reaction Mechanisms in Organometallic Chemistry and Catalysis

Received: April 9, 2024 Revised: July 26, 2024 Accepted: August 13, 2024



Scheme 1. Previous Work on Nucleophilic Cp Ring Activation, and the Focus of This Work



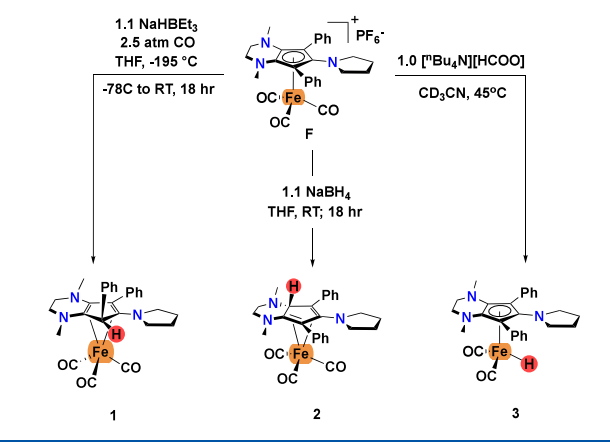
We recently determined that amine-rich CpN3 ligands with the general formula  $[Cp^{N3}Fe(CO)_2(NCMe)]^+$  are active  $H_2$ production electrocatalysts in the presence of exogenous acid. 19,20 Mechanistic studies revealed that exogenous acid selectively protonates the CpN3 ring in the endo position, and this transient intermediate rapidly generates an Fe-H complex under reducing conditions via ligand-to-metal proton migration. To experimentally support the formation of an endo-Cp<sup>N3</sup>H intermediate during catalysis, the model complex (endo-Cp<sup>N3</sup>H)Fe(CO)<sub>3</sub> (1) was independently synthesized via reduction of [(Cp<sup>N3</sup>)Fe(CO)<sub>3</sub>]<sup>+</sup> (F) using the strong hydride donor NaHBEt<sub>3</sub> (Scheme 1).<sup>20</sup> Although low temperatures and elevated pressures of CO were needed to form the product in reasonable yield, the mechanism of H<sup>-</sup> addition to generate 1 remained unclear. The kinetic and thermodynamic C-H hydricities of 1 also remained unknown, motivating us to consider that the  $\eta^4$ -Cp<sup>N3</sup>H motif might be useful as a conduit for transferring H<sup>-</sup> to substrates such as CO<sub>2</sub>, especially if the thermodynamic hydricity ( $\Delta G^{\circ}_{H-}$ ) was found to be less than 44 kcal/mol in acetonitrile. <sup>14,21,22</sup>

Herein, we study the divergent mechanistic pathways toward the formation of three different Fe complexes: an endo hydride addition product (1),<sup>20</sup> an exo hydride addition product (2), and an Fe-H complex (3), 20 all of which can be accessed from starting material F by simply changing the hydride reagent used (Scheme 1). We also show that the experimental hydricities for 1 and 2 are not accessible via equilibrium hydricity measurements for kinetic reasons, even though DFT calculations predict that their thermodynamic hydricities  $(\Delta G^{\circ}_{H^{-}})$  are amenable to thermochemical equilibrium measurements (51.0 and 49.4 kcal/mol, respectively). In studying the mechanism of formation for complexes 1 and 3, kinetic studies reveal that the rate-limiting formation of iron formyl intermediates is in excellent agreement with theory. However, subsequent  $\alpha$ -H elimination pathways are found to be prohibitively high, suggesting that the H transfer mechanism(s) involved are more convoluted than initially expected.

#### RESULTS AND DISCUSSION

The salt  $[(Cp^{N3})Fe(CO)_3][PF_6]$  (F) was prepared as previously published. In the Experimental Section, we provide a modified protocol for synthesizing the ligand synthon 4-hydroxy-2,5-diphenylcyclopentane-1,3-dione. The Supporting Information includes a solid-state structure of free ligand  $[Cp^{N3}][B(C_6F_5)_4]$ . We previously reported that synthesis of  $(endo-Cp^{N3}H)Fe(CO)_3$  (1) is performed under 2.5 atm of CO and requires addition of the CO prior to addition of NaHBEt<sub>3</sub> to the reaction mixture (Scheme 2).  $^{20}$ 

Scheme 2. Reactivity of F with Hydride Donors



This is performed via cryogenic condensation of CO followed by addition of NaHBEt3 under a stream of nitrogen. Under these conditions, the reaction mixture remains pumpkin orange, and upon workup and crystallization it gives a 35% yield of 1. Without the addition of CO, uncontrolled decomposition is observed, producing a green-brown reaction mixture with trace amounts of  $Cp^{N3}FeH(CO)_2$  (3). To alleviate the need for low-temperature conditions and excess CO, we sought an alternative method to access 1 by surveying its reactivity with milder hydride donors. Thus, we used NaBH<sub>4</sub> under nitrogen at room temperature, and the color remained lemon yellow over the course of the reaction. The unique <sup>1</sup>H NMR signal at 4.76 ppm in C<sub>6</sub>D<sub>6</sub> corresponding to the CpH proton of 1 was not observed, and a new singlet at 3.92 ppm appeared. To our surprise, single crystals suitable for X-ray diffraction revealed that exo attack at a different CpN3 position had occurred, producing (exo-Cp<sup>N3</sup>H)Fe(CO)<sub>3</sub> (2) in 56% isolated yield (Figure 1).

X-ray crystallographic characterization of 2 reveals structural similarities to 1. Bond lengths along the unsaturated portion of

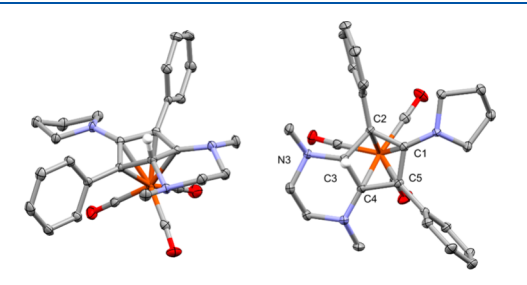


**Figure 1.** X-ray crystallographic structure of **2** with 50% probability ellipsoids (most hydrogens omitted for clarity). A top-down image is shown on the right with atom labels; see discussion for relevant bond lengths.

the  $\eta^4$ -Cp group (C1–C2 = 1.452(2) Å, C1–C5 = 1.440(3) Å, C4–C5 = 1.441(2) Å) are within a typical range for conjugated C(sp²)–C(sp²) systems, while the C–C bonds to tetrahedral C3 are elongated (C2–C3 = 1.537(2) Å; C4–C3 = 1.521(3) Å) into the expected range for C(sp²)–C(sp³) bonds. C(sp²)–C(sp³) bonds. C(sp²)–C(sp³) bonds bonding from the formally Fe(0) center. The C–N bond connected to tetrahedral C3 (C3–N3 = 1.459(2) Å) is significantly elongated relative to the other C–N bonds (C4–N2 = 1.388(2) Å; C1–N1 1.378(2) Å), indicating a break in delocalization and putting the C3–N3 into the range for a C(sp³)–N(sp³) bond. C(sp³)–N(sp³) bond.

To probe the oxidative stabilities of 1 and 2, cyclic voltammetry (CV) experiments in the anodic direction reveal that the oxidation of 1 complex shows a redox wave at scan rates  $\geq$  30 V/s ( $E_{1/2}$  = 0.27 V; Table 1). The oxidation of

Table 1. Computed Hydricities and Experimentally Determined Potentials via Cyclic Voltammetry

complex	$\Delta G_{\mathrm{H-}}  (\mathrm{kcal}  \mathrm{mol}^{-1})^a$	$E \left( V \text{ vs } Fc^{+/0} \right)^{b}$
1	51.0	$-0.27 (E_{1/2})^c$
2	49.4	$0.20 (E_{pa})^c$
3	53.9	$0.00 (E_{pa})^{20}$

<sup>a</sup>Computed relative to the hydricity of BIMH in acetonitrile at the ωB97X-V<sup>28</sup>/def2-QZVPP<sup>29</sup>+COSMO-RS(MeCN)<sup>30,31</sup>//r<sup>2</sup>SCAN-3c<sup>32</sup>+COSMO(MeCN)<sup>33</sup> level of theory. <sup>b</sup>Conditions: N<sub>2</sub>, MeCN, 0.1 M [Bu<sub>4</sub>N][PF<sub>6</sub>], 1.0 mM analyte. See the SI for voltammograms. <sup>c</sup>Measured at 30 V/s.

complex 2 remains irreversible, even at high scan rates ( $E_{\rm pa}$  = 0.20 V), which is analogous to hydride complex 1. In all three cases, GC analysis reveals that ca. 1 equiv of CO is released, suggestive of product decomposition.

Next, we surveyed the reactivity of 1 and 2 with hydride acceptors both computationally and experimentally (see the SI for the computational isodesmic schemes employed). Quantifying hydricities (hydride donor abilities;  $\Delta G_{H-}$ ) via thermochemical equilibrium measurements provides valuable information about the capability of molecules to transfer Hmoieties in stoichiometric and catalytic transformations. 14,25 Computational modeling indicates that  $\Delta G_{H-}(1) = 51.0$  kcal  $\text{mol}^{-1}$  and  $\Delta G_{\text{H-}}(2) = 49.4 \text{ kcal mol}^{-1}$  (Table 1), which are computed relative to the known hydricity of 1,3-dimethyl-2phenylbenzimidazole (BIMH) in acetonitrile ( $\Delta G_{H-}$ = 50.1 kcal/mol).<sup>26</sup> Based on the computed hydricity of 2, we chose 1,2,3,5,6-pentamethylbenzimidazole (Me<sub>5</sub>BzImH;  $\Delta G_{H-}$  = 43.0 kcal mol<sup>-1</sup>)<sup>27</sup> as the hydride donor, which should favorably transfer  $\mathrm{H}^-$  to  $\mathrm{F}$  on thermochemical grounds ( $\Delta G_{\mathrm{rxn}}$ = -6.4 kcal/mol; Figure 2).

Surprisingly, no reaction between F and Me<sub>5</sub>BzImH was observed, and for the sake of completion, mixing the 1,2,3,5,6-pentamethylbenzimidazolium salt [Me<sub>5</sub>BzIm][B(C<sub>6</sub>F<sub>5</sub>)<sub>4</sub>] with 2 elicited no reaction (the B(C<sub>6</sub>F<sub>5</sub>)<sub>4</sub><sup>-</sup> variant was prepared to facilitate solubility in acetonitrile; see the Exerimental Section for details). Similar experiments were performed using F, 1, BIMH, and [BIM][B(C<sub>6</sub>F<sub>5</sub>)<sub>4</sub>], and again, no equilibration was observed from either direction. Since these ground state thermochemical measurements were unsuccessful, we hypothesized that the significant steric bulk surrounding the *endo-* and *exo-*Cp<sup>N3</sup>H positions might inhibit hydride transfer, and DFT modeling with 1 validates that the hydride transfer transition

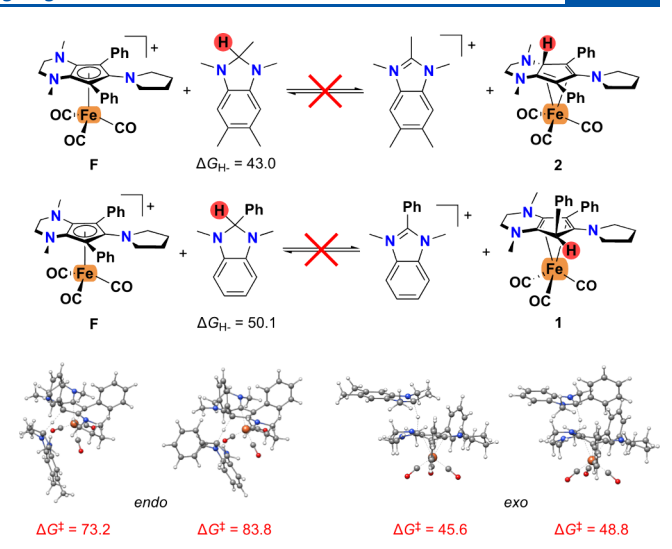


Figure 2. (Top) Attempted equilibration experiments with hydride donors and acceptors along with hydricities for BIMH and  $Me_3BzImH$ . (Bottom) Transition state structures and free energies for the reaction of BIMH and  $Me_3BzImH$  with  $[(Cp^{N3})Fe(CO)_3]^+$  (F) to generate 1 or 2. All energies are given in kcal/mol.

states to the *endo* and *exo* positions are massive ( $\Delta G^{\ddagger} = 73.2$  and 83.8 kcal mol<sup>-1</sup> for endo,  $\Delta G^{\ddagger} = 45.6$  and 48.8 kcal mol<sup>-1</sup> for exo), barring us from obtaining experimental hydricities (Figure 2, bottom).

After establishing that sluggish kinetic hydricities were preventing us from using benzimidazolium salts for equilibrium measurements, we shifted to using formate (HCOO<sup>-</sup>), a sterically unencumbered hydride donor that might smoothly transfer  $H^-$  to the  $Cp^{N3}$  ring ( $\Delta G_{H^-}=44$  kcal mol<sup>-1</sup>, MeCN). In a J. Young NMR tube, ["Bu4N][HCOO] was combined with F in CD<sub>3</sub>CN, and no reaction was observed at room temperature. Heating the sample to 45 °C for 20 h cleanly produced a product with a characteristic singlet at -10.72 ppm via <sup>1</sup>H NMR spectroscopy, corresponding to CpN3FeH(CO)<sub>2</sub> (3) in solution (Scheme 2). Based on the computed hydricity of 53.9 kcal/mol for 3 (Table 1), this result is consistent with the liberation of CO<sub>2</sub> over the course of the reaction. However, prolonged heating also leads to gradual decomposition, and black insoluble crystals suitable for X-ray diffraction consistently form at the bottom of unstirred reaction vessels. These black crystals correspond to the dimeric decomposition product  $(Cp^{N2}Fe(CO)_2)_2$  (4, Scheme 3). The fate of the pyrrolidine moiety remains unclear. Due the poor solubility of 4 in common organic solvents, characterization was limited to IR spectroscopy with CO stretches at 1921 and 1730 cm<sup>-1</sup> for the terminal and bridging carbonyls, respectively. Importantly, the formation of ring-activated products 1 or 2 was not spectroscopically observed via <sup>1</sup>H NMR during the reaction.

Flummoxed by the divergent outcomes upon reacting F with different hydride donors, we sought to obtain more information about initial hydride attack in the presence of HBEt<sub>3</sub><sup>-</sup>, HCOO<sup>-</sup>, and BH<sub>4</sub><sup>-</sup> as shown in Figure 3. Based on the calculated hydricities at standard state conditions in MeCN, all three hydride donors are hydridic enough to form complexes 1-3 (see Table S1). To mirror the experimental conditions used, reactions with HBEt<sub>3</sub><sup>-</sup> and BH<sub>4</sub><sup>-</sup> are modeled at 25 °C in THF while reactions with HCOO<sup>-</sup> are modeled at 45 °C in MeCN. The elevated temperature increases the

Scheme 3. Reaction of F with [NBu<sup>n</sup><sub>4</sub>][HCOO], and Molecular Structure of 4<sup>a</sup>

<sup>a</sup>Structure shown with 50% probability ellipsoids, and hydrogens omitted for clarity.

reaction free energy barriers with HCOO<sup>-</sup>, since the entropy penalty of the transition states (two particles form one in the TS) is increased. Also, THF is less polar than MeCN, which stabilizes the ionic reactants less but results in more exothermic reaction free energies and smaller barriers to generate products with net neutral charges. DFT calculations reveal that direct hydride transfer to the endo position is insurmountable with all reagents, as the free energy barriers range from 54.2 to 60.4 kcal/mol (Figure 3a). Therefore, hydride donor sterics are *not* a factor, as hypothesized in our reactions with Me<sub>5</sub>BzImH and BIMH. Direct hydride transfer to form *exo* product 2 is kinetically accessible with HBEt<sub>3</sub><sup>-</sup> and BH<sub>4</sub><sup>-</sup> (Figure 3b), while the barrier for HCOO<sup>-</sup> addition is highest, even at 45 °C ( $\Delta G^{\ddagger} = 27.3 \text{ kcal/mol}$ ). In line with experiment, the barrier for BH<sub>4</sub><sup>-</sup> attack in the *exo* position is most favorable ( $\Delta G^{\ddagger} = 14.8 \text{ kcal/mol}$ ).

The most favorable reaction pathways are HBEt3 or HCOO<sup>-</sup> attack on CO to generate iron formyl intermediate 5 (Figure 3c;  $\Delta G^{\ddagger} = 7.4$  and 25.6 kcal/mol, respectively). Unfortunately, a true transition state could not be located for BH<sub>4</sub> addition to generate 5 since the saddle point on the minimal energy pathway is flat and its transition state optimizations ran either into the reactants or into the product. The reaction free energy for BH<sub>4</sub><sup>-</sup> addition to generate 5 is endothermic ( $\Delta G = 19.3 \text{ kcal/mol}$ ) and remains so even after considering BH<sub>3</sub> dimerization ( $\Delta G = 4.5 \text{ kcal/mol}$ ) and is therefore unfeasible. Finally, direct attack of HCOO or BH<sub>4</sub> on the metal center to form hydride complex 6 is also energetically unfeasible (Figure 3d). Therefore, these computational data signify that direct hydride attack to make 1 or 6 is not operative, and generation of complexes 1 and 3 proceeds via initial formation of iron formyl intermediate 5 in the presence of HCOO- and HBEt3-.

The effects of the spin state and multireference character have also been computationally probed. We performed single-point calculations for the ground states and transition states shown in Figure 3 on the high-spin triplet state with three different hybrid DFT methods that employ varying amount of Hartree–Fock-like exchange. All spin splittings are larger than 5 kcal/mol (and often much larger; see Table S2). Therefore, our assumption that all species are in a low-spin ground state appears to be justified. To investigate whether multireference

character is of importance, we employed fractional occupation number weighted density (FOD) analysis <sup>34</sup> for  $TS_{F,5}$  with  $R = CO_2$  (Figure S11). Since the FOD is mostly centered on the iron atom and the integrated  $N_{FOD}$  value is relatively small ( $N_{FOD} = 0.45$ ), multireference character seems to be unproblematic.

The relatively straightforward reaction conditions to synthesize 3 using HCOO are amenable to reaction monitoring via NMR spectroscopy with the hopes of spectroscopically identifying iron formyl intermediate 5 via hydride transfer from HCOO-. The synthesis and reactivity of iron formyl intermediates has been reported in detail by Astruc upon reacting  $[Cp*Fe(CO)_2R]^+$  (R = CO, PMe<sub>3</sub>, PBu<sub>3</sub>, PPh<sub>3</sub>) with 1 equiv of NaBH<sub>4</sub> at temperatures  $\leq -30$  °C; however, these complexes are all unstable at room temperature. 13 In a J. Young NMR tube, F was combined with 1 equiv of [NBun4][HCOO] in CD3CN, and the vessel was pressurized with 6.5 atm (95 psi) of CO to inhibit the formation of hydride complex 3. The weakly coordinating NBu<sub>4</sub><sup>+</sup> was specifically chosen in order to minimize the influence of countercation participation during the course of the reaction. 13 In addition to a <sup>1</sup>H NMR signal at 8.02 ppm for [NBu<sup>n</sup><sub>4</sub>][HCOO], we observe the appearance of a broad <sup>1</sup>H NMR signal at 9.41 ppm, assigned to be the formyl proton for intermediate 5 (Figure 4, top).

We also sought to understand the influence of BEt3 on the formation of formyl intermediate 5. First, we performed a reaction under 6.5 atm of CO with 1 equiv of [NBu<sup>n</sup><sub>4</sub>] [HCOO], and <sup>1</sup>H NMR spectroscopic analysis indicated the presence of 5. Then, the J. Young NMR tube was vented under an N2 atmosphere, 1 equiv of BEt3 was quickly added, and the tube was again pressurized to 6.5 atm of CO. <sup>1</sup>H NMR spectroscopic analysis reveals 5·BEt3, with a sharp deshielded multiplet at 9.69 ppm due to <sup>1</sup>H-<sup>11</sup>B coupling (Figure 4, bottom). Although it was difficult to obtain well-resolved <sup>13</sup>C NMR spectral data of the carbonyl/formyl resonances for 5 and 5·BEt<sub>3</sub>, <sup>1</sup>H-<sup>13</sup>C HSQC on 5·BEt<sub>3</sub> reveals a cross-peak at 207.7 ppm for the formyl carbon, solidifying our peak assignment (Figure S3). This chemical shift contrasts dramatically with the <sup>13</sup>C NMR assignment of the deshielded formyl carbon atom in Cp\*Fe(CO)(CHO)(PBu<sub>3</sub>) (306.5 ppm), 13 underscoring the strong electron donor properties of Cp<sup>N3</sup> ligands. 19

We then studied the kinetics of the formation of 3 in the presence of [NBu<sup>n</sup><sub>4</sub>][HCOO]. By utilizing the method of initial rates, we observe a linear dependence when varying the initial concentrations of [(Cp<sup>N3</sup>)Fe(CO)<sub>3</sub>]<sup>+</sup> (F) or [<sup>n</sup>Bu<sub>4</sub>N]-[HCOO] and monitoring the reaction rates by <sup>1</sup>H NMR spectroscopy (Figure 5 and Figure S6). In both cases, log-log plots indicate a first-order dependence on the concentration of F and  $[^{n}Bu_{4}N][HCOO]$ , thereby giving the following rate law, where Fe is the tricarbonyl complex F: rate =  $k[Fe][HCOO^{-}]$ . To observe the effects of isotopic substitution on the reaction rate, we ran reactions under pseudo-first-order conditions by using an excess of [NBu<sup>n</sup><sub>4</sub>][HCOO] or [NBu<sup>n</sup><sub>4</sub>][DCOO] at 45 °C and monitored by <sup>1</sup>H NMR spectroscopy (Figure 6). The rate of formation of 3 was found to be  $3.0 \pm 0.1 \times 10^{-5}$ s<sup>-1</sup>, and the rate of formation of the deuterated analogue 3-D was found to be  $1.9 \pm 0.1 \times 10^{-5} \text{ s}^{-1}$ , with  $k_{\rm H}/k_{\rm D} = 1.8$ . This kinetic isotope effect (KIE) is comparable to primary kinetic isotope effects involving formate-centered hydride transfers in Mo-containing formate dehydrogenase  $(k_H/k_D = 2.44)^{.38}$ Table 2 compares the kinetic data between experiment and

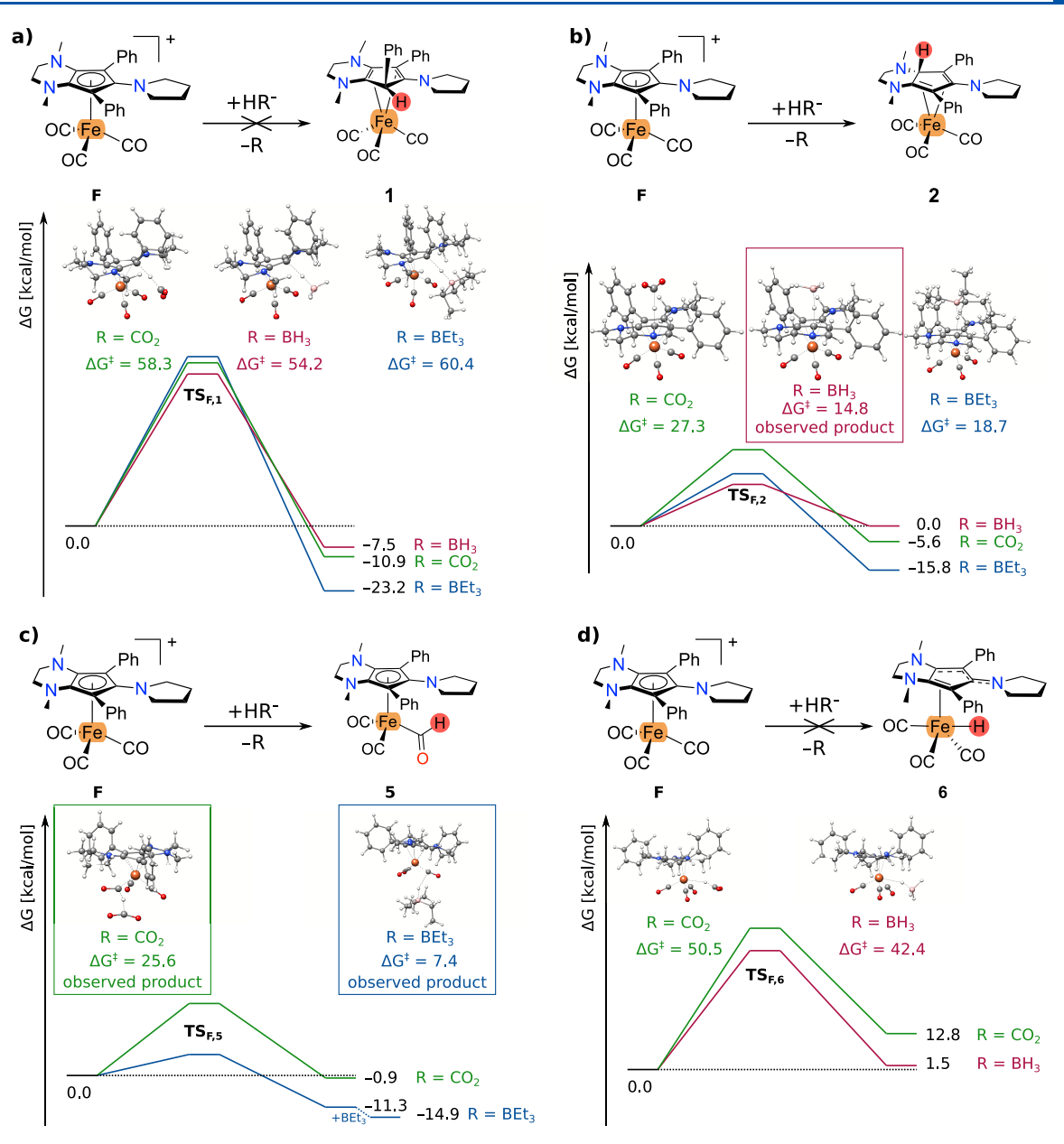
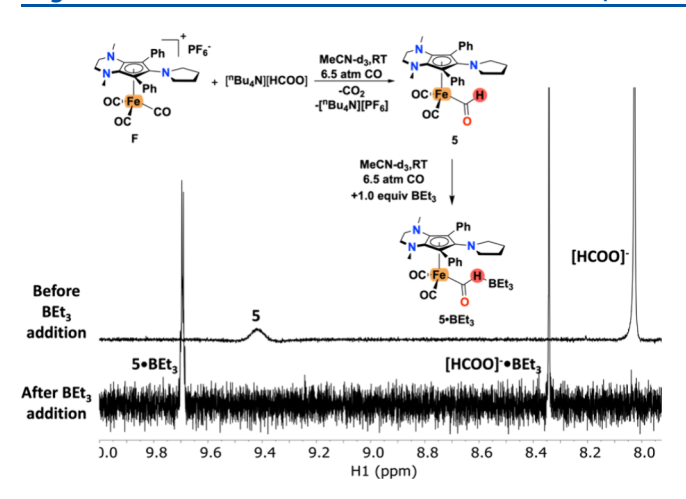


Figure 3. DFT-computed free energy profiles on the ωB97X-V/def2-QZVPP+COSMO-RS level of theory of hydride addition to generate an *endo*-Cp<sup>N3</sup>H intermediate (a), *exo*-Cp<sup>N3</sup>H intermediate (b), formyl intermediate (c), or hydride adduct (d) via reaction with HCOO<sup>-</sup> HBEt<sub>3</sub><sup>-</sup> or BH<sub>4</sub><sup>-</sup>. Energies are given in kcal/mol. Implicit solvation for THF is used with HBEt<sub>3</sub><sup>-</sup> and BH<sub>4</sub><sup>-</sup>, and implicit MeCN solvation is used with HCOO<sup>-</sup>. Reactions involving HCOO<sup>-</sup> were modeled at 45 °C, while all others were modeled at 25 °C.

theory, and all values are in excellent agreement, indicating that  $TS_{F,5}$  is rate limiting during the formation of 3.

So far, our combined experimental and computational data to generate 3 via HCOO<sup>-</sup> are consistent with the formation of formyl intermediate 5. The following question remains: how does Fe–H complex 3 form when using HCOO<sup>-</sup> and how does *endo*-Cp<sup>N3</sup>H adduct 1 form in the presence of HBEt<sub>3</sub><sup>-</sup>? Thus far, our data suggests that the formation of 1 and 3 occurs via formation of 5·BEt<sub>3</sub> and 5, respectively, and we modeled several different intramolecular rearrangements starting from these molecules. Surprisingly, all computed pathways were prohibitively high, and the key transition states are shown in Figure 7 (complete reaction pathways are shown in Figures S9 and S10). Starting from 5,  $\alpha$ -H elimination from the formyl ligand with concomitant CO dissociation (TS<sub>5,3</sub>) has a barrier of 40.4 kcal/mol in MeCN while  $\alpha$ -H elimination

without CO dissociation has a barrier of 30.0 kcal/mol ( $TS_{5,6}$ ). Stepwise CO dissociation followed by  $\alpha$ -H elimination is also prohibitively high ( $TS_{7,3} = 39.3 \text{ kcal/mol}$ ). Starting from formyl intermediate  $5 \cdot BEt_3$ , direct H migration to the *endo-*Cp<sup>N3</sup> ring to form 1 has a TS free energy of 67.5 kcal/mol in THF ( $TS_{5BEt3,1}$ ). Dissociation of BEt<sub>3</sub> followed by direct H migration to the *endo-*Cp<sup>N3</sup> ring is also unfavorable (59.3 kcal/mol;  $TS_{5,1}$ ). Potential lower lying high-spin states were investigated by calculations of vertical singlet—triplet spin splittings (see Table S3), which suggest that no lower lying high-spin transition states are present. These computational data suggest that implicit solvation, bimetallic reaction pathways, or a combination of both may play important roles in the formation of 1 and 3.



**Figure 4.** (Top) Reactivity of F with [NBu<sup>n</sup><sub>4</sub>][HCOO] and BEt<sub>3</sub> under a CO atmosphere to generate 5 and 5·BEt<sub>3</sub>. (Bottom) <sup>1</sup>H NMR spectral data showing the formyl resonances of 5 and 5·BEt<sub>3</sub>.

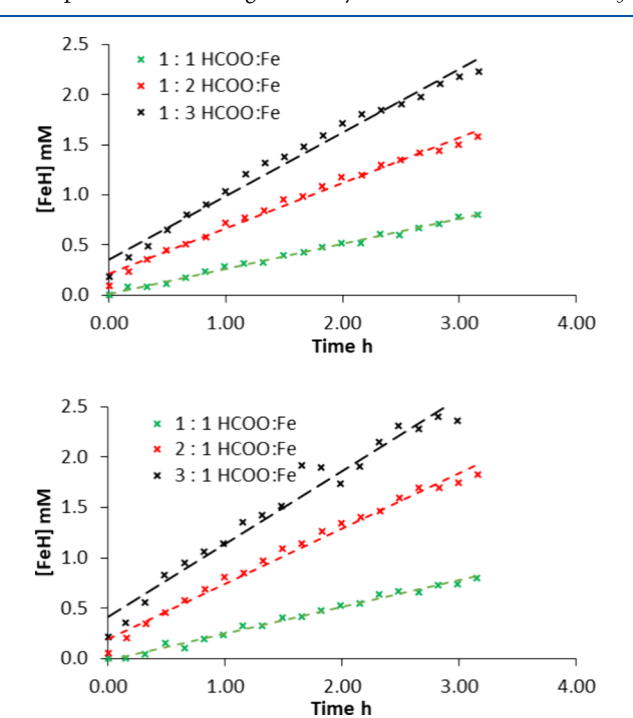
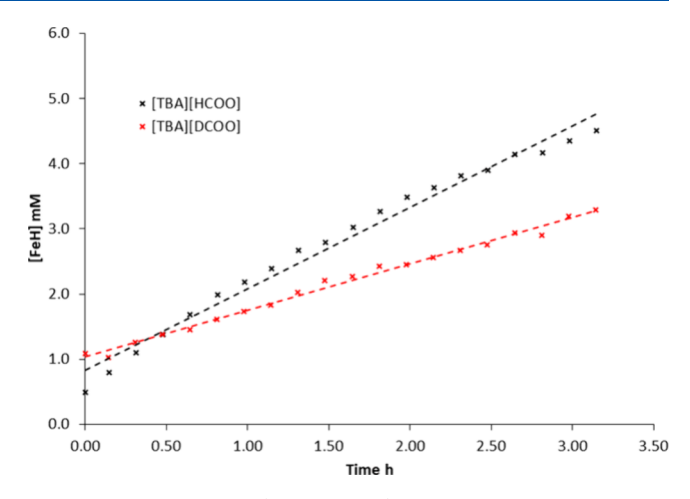


Figure 5. Kinetic traces for the conversion of 1 to 3 in CD $_3$ CN at 45 °C. (Top) Varying the initial concentration of 1 (12.6, 26.8, and 38.4 mM) with a constant initial concentration of [NBu $^n$  $_4$ ][HCOO] (18.5 mM). (Bottom) Varying the initial concentration of [NBu $^n$  $_4$ ] [HCOO] (14.8, 29.6, and 41.0 mM) with a constant initial concentration of 1 (15.9 mM).

#### CONCLUSIONS

In this report, we sought to further explore the ring activation chemistry of the tricarbonyl iron complex  $[(Cp^{N3})Fe(CO)_3]^+$  (F). Our previous work demonstrated the synthesis of an *endo-*Cp<sup>N3</sup>H addition product (1) via hydride addition to the chemically noninnocent Cp<sup>N3</sup> ligand using NaHBEt<sub>3</sub>. In search of more user-friendly reaction conditions, we serendipitously discovered that the weaker hydride donor NaBH<sub>4</sub> forms an *exo-*Cp<sup>N3</sup>H addition product (2). Moreover, using HCOO as the hydride donor furnishes a known FeH complex (3) which decomposes with prolonged heating.



**Figure 6.** Kinetic traces (first-order fit) for the conversion of **F** to **1** (black) and **1-D** (red) in CD<sub>3</sub>CN at 45 °C using [TBA][HCOO] and [TBA][DCOO], respectively.

Table 2. Kinetics Data for the Reaction of F To Generate 3 via [NBu<sup>n</sup><sub>4</sub>][HCOO] or [NBu<sup>n</sup><sub>4</sub>][HCOO] at 45 °C

	experiment	DFT $(TS_{F,5})^a$		
$k (s^{-1})$	$3.0 \pm 0.1 \times 10^{-5}$	$1.70 \times 10^{-5}$		
$\Delta G^{\ddagger}_{318}$ (kcal/mol)	25.2	25.6		
$k_{ m H}/k_{ m D}$	1.8	1.8		
<sup>a</sup> See Table 1 for level of theory.				

TS<sub>5,3</sub> TS<sub>5,6</sub> TS<sub>7,3</sub> 39.3

40.4 53.8 30.0 30.9 39.3

TS<sub>5,6</sub> TS<sub>7,3</sub> 39.3

**Figure 7.** DFT-computed TS barriers for high-energy pathways that were considered after formation of  $5 \cdot \mathrm{BEt_3}$  and  $5 \cdot \mathrm{Free}$  energies are given in kcal/mol relative to 5 for numbers in black and  $5 \cdot \mathrm{BEt_3}$  for numbers in blue. Free energies in blue are modeled in THF at  $25 \, ^{\circ}\mathrm{C}$ , and free energies in black are modeled in acetonitrile at  $45 \, ^{\circ}\mathrm{C}$ .

59.3

The impact of the hydride donor on the regioselectivity of these hydride transfers led us to undertake mechanistic studies. In an attempt to differentiate the site selectivity of the hydride transfer on thermodynamic grounds, we sought to experimentally measure the hydricities of  $(endo\text{-}Cp^{N3}\text{H})\text{Fe}(CO)_3$  (1) and  $(exo\text{-}Cp^{N3}\text{H})\text{Fe}(CO)_3$  (2). The prohibitively sluggish kinetic hydricities of 1 and 2 led to no reaction in the presence of hydride acceptors, as supported by experiment and DFT calculations. We then undertook a guided experimental and computational study to help explain their reactivity with different hydride donors. Formation of 2 likely occurs via direct hydride transfer to the exo position with NaBH<sub>4</sub>, and direct hydride attack with exogenous hydride donors to give 1 and 3 can be excluded due to massive DFT-computed

transition state free energies. Based on kinetic data, there is an overall second-order rate law for rate-determining hydride transfer with HCOO<sup>-</sup>, which is in excellent agreement with DFT calculations. We were able to observe an iron formyl intermediate (5) via <sup>1</sup>H NMR spectroscopy, and addition of the Lewis acid BEt<sub>3</sub> improved spectral resolution to form the adduct 5·BEt<sub>3</sub>, which is a likely intermediate en route to *endo*-Cp<sup>N3</sup>H adduct 1. While it was challenging to rationalize the mechanisms of formation for the experimentally isolated 1 and FeH complex 3, state-of-the-art DFT calculations were valuable to rule out several potential rearrangement pathways. Collectively, this synergistic computational and experimental mechanistic study highlights the unexpected subtleties of exogenous hydride selectivity with FeCp<sup>N3</sup> complexes, and we continue to explore the unique reactivity patterns of Cp<sup>N3</sup> ligands coordinated to transition metals.

# **EXPERIMENTAL SECTION**

General Comments. All reactions were carried out under an atmosphere of nitrogen or argon using standard glovebox or highvacuum line (Schlenk) techniques unless stated otherwise. All reagents and solvents were stored in a nitrogen-filled glovebox prior to use unless stated otherwise. Acetonitrile and pentane were dried and degassed over activated alumina using an IT/Inert solvent purification system. Additionally, THF, acetonitrile, and toluene were dried over 20% w/v activated 3 Å molecular sieves. CD<sub>3</sub>CN and C<sub>6</sub>D<sub>6</sub> were subjected to three freeze-pump-thaw cycles and dried over 10% w/v activated 3 Å molecular sieves in a glovebox.<sup>36</sup> Glassware was dried overnight at 140 °C and cooled under dynamic vacuum in a glovebox antechamber. Infrared spectra were recorded on a Thermo Nicolet FT-IR instrument by preparing a KBr pellet or ATR cell. Elemental analyses were run by the CENTC Elemental Analysis Facility, Department of Chemistry, University of Rochester. Microanalysis samples were weighed with a PerkinElmer model AD6000 Autobalance, and their composition was determined with a PerkinElmer 2400 Series II Analyzer. Infrared spectra were recorded on a Thermo Nicolet FT-IR instrument. 1,4-Dimethyl-5,7-dipheny- $\label{eq:constant} $$ \operatorname{loctahydro-6H-cyclopenta[b]pyrazin-6-one, [Cp^{N3}][BF_4],}^{19} [(Cp^{N3})-Fe(CO)_3][PF_6] (F),\\ {}^{19,20} (endo-Cp^{N3}H)Fe(CO)_3 (1),\\ {}^{20} Cp^{N3}FeH-(CO)_2 (3),\\ {}^{20} [^nBu_4N][HCOO],\\ {}^{37} [Me_3BzIm][I],\\ {}^{27} and [BIM][I]^{38}$ were synthesized according to previously published procedures and matched published spectroscopic data. The salts [Me<sub>5</sub>BzIm][B- $(C_6F_5)_4]$  and  $[BIM][B(C_6F_5)_4]$  were prepared by ion exchange of  $[Me_5BzIm][I]$  and [BIM][I] with  $[K][B(C_6F_5)_4]$  in diethyl ether followed by filtration using a 0.4 µm PTFE syringe filter and drying under high vacuum. The compounds were used without further

NMR. <sup>1</sup>H and <sup>13</sup>C NMR spectra were collected on a Bruker Avance III 500 MHz NMR with autosampler capability using either a 5 mm BBO broadband probe or 5 mm BBFO broadband probe. NMR spectra were referenced internally to residual <sup>1</sup>H and <sup>13</sup>C signals in the deuterated solvent. Deuterated solvents were degassed via three freeze–pump—thaw cycles and dried over 10% w/v activated 3 Å molecular sieves in a nitrogen-filled glovebox.

To determine the reaction order for the formation of 3 in the presence of  $[NBu^n_4][HCOO]$ , stock solutions of complex F and  $[^nBu_4N][HCOO]$  (or  $[^nBu_4N][DCOO])$  were prepared in  $CD_3CN$ . The samples were diluted to a total volume of 0.5 mL in a J. Young tube and added to an NMR probe heated to 45 °C. Spectra were automatically collected every 10 min. The concentration of reagents was determined by integrating the peak at 3.13 ppm  $(^nBu_4N^+)$  and assuming the initial concentration of  $^nBu_4N^+$  was equal to the initial concentration of  $[^nBu_4N][HCOO]$ . The initial ratio of F:HCOO—was determined using the integrations of the peaks at 3.13 and 2.21 ppm (F) in the first spectrum collected. The concentration of the final product was determined using the integration of the peak at -11.19 ppm (FeH) at all time points.

**X-ray Diffraction.** Single crystals were mounted on a nylon loop and cooled to 100 K under a dry nitrogen stream before data collection unless otherwise stated. SCXRD was performed on a Rigaku XtaLAB Synergy-I diffractometer using Cu K $\alpha$  with a HyPIX HPC detector. Structures were refined by full-matrix least-squares based on F2 with all reflections (SHELXTL V5.10; G. Sheldrick, Siemens XRD, Madison, WI). Non-hydrogen atoms were refined with anisotropic displacement coefficients, and hydrogen atoms were treated as idealized contribution. SADABS (Sheldrick, 12 G.M. SADABS (2.01), Bruker/Siemens Area Detector Absorption Correction Program; Bruker AXS: Madison, WI, 1998) absorption correction was applied. Crystallographic data has been deposited with the Cambridge Crystallographic Data Center and is available free of charge through the CCDC online database.

4-Hydroxy-2,5-diphenylcyclopentane-1,3-dione. This known compound was synthesized using a modified procedure which avoids the use of sodium metal. 39,40 A stoppered Schlenk flask was charged with 25 mL of absolute ethanol, which had been dried overnight over 20% w/v activated molecular sieves under a blanket of nitrogen. The liquids were transferred via syringe to an air-free Schlenk flask. Under a dynamic stream of nitrogen, sodium ethoxide powder (47.5 mmol, 3.24 g, 2.0 equiv) was added, and the solution was vigorously stirred until the NaOEt dissolved. Then, 1,3-diphenyl-2-propanone (23.8) mmol, 5.00 g, 1.0 equiv) and diethyl oxalate (23.8 mmol, 3.49 g, 1.0 equiv) were weighed on the benchtop and added to the solution. Upon addition of these reagents, the reaction mixture turned orange. The reaction was stirred for 2 h at room temperature under inert gas, during which the reaction mixture changed color from orange to purple. At this point, the reaction was moved to an ice bath and cooled to 0 °C, and the remaining workup was conducted under air. Glacial acetic acid was added dropwise until equimolar amounts of  $\mbox{[K][B(C_6F_5)_4]}$  and  $\mbox{[Cp$^{N3}][BF_4]}\mbox{\ \ were dissolved in a minimum}$ amount of diethyl ether, giving a white precipitate suspended in a blue solution. This suspension was filtered with a PTFE syringe filter giving a blue solution, which was layered with pentane and stored at −30 °C in a glovebox freezer. Overnight, a viscus blue oil formed on the bottom of the vial, and after several weeks at -30 °C, this oil crystallized, giving X-ray-quality crystals (Figure S12). This product was not characterized any further; pH  $\approx 7$  was measured with pH test strips. At this point, a yellow precipitate began to form, and the complete reaction was transferred to a beaker containing ca. 50 g of ice. The reaction was further acidified by dropwise addition of concentrated sulfuric acid until the pH measured ~1. During this time, more yellow precipitate formed. The yellow precipitate was collected on a medium-pore glass filter frit, transferred to a roundbottom flask, and dried overnight under high vacuum. Redissolving the product in a minimal amount of acetone followed by addition of hexanes precipitates a light-yellow microcrystalline product in 90% yield (5.69 g) and matches previously published spectroscopic data. (exo-Cp<sup>N3</sup>H)Fe(CO)<sub>3</sub> (2). In a glovebox, [(Cp<sup>N3</sup>)Fe(CO)<sub>3</sub>][PF<sub>6</sub>]

(F) (122 mg, 186  $\mu$ mol, 1.0 equiv) was dissolved in THF (3 mL). To this solution was added LiAlH<sub>4</sub> (45 mg, 1.19 mmol), and the yellow solution was stirred for 18 h at room temperature. The solvent was removed under high vacuum; the residue was dissolved in a minimum amount diethyl ether (ca. 4 mL) and filtered using a 0.45  $\mu$ m Teflon syringe filter. The red-orange solution was layered with pentane (ca. 12 mL) and cooled to -35 °C in a glovebox freezer until crystals formed. The mother liquor was decanted, and the crystals were washed with pentane  $(3 \times 1 \text{ mL})$  and dried under high vacuum to give 2 as a yellow crystalline solid (53 mg, 56%). These crystals were suitable for X-ray analysis.  $^{1}$ H NMR (500 MHz, CD<sub>3</sub>CN)  $\delta$  7.71 (s, 3H, broad, Arom), 7.54 (s, 2H), 7.48-7.36 (m, 2H, Arom.), 7.36-7.05 (m, 3H, Arom), 3.88 (s, 1H, CpH), 2.70-2.48 (m, 4H, overlapping, en), 2.22-2.10 (m, 4H, overlapping, Pyrr), 1.57 (s, 3H, Me), 1.54 (s, 3H, Me), 1.36-1.28 (m, 4H overlapping, Pyrr). <sup>13</sup>C NMR (126 MHz, CD3CN)  $\delta$  219.15 (3 CO), 144.21(1 Arom), 136.33 (1 Arom), 134.35 (1 Arom), 129.72 (2 Arom), 129.11 (2 Arom), 128.72 (1 Arom), 128.63 (1 Arom), 127.92 (1 Arom), 116.45 (Cp), 104.57 (Cp), 97.51 (Cp), 73.75 (Cp), 67.00 (2 CH<sub>2</sub> Pyrr), 52.65 (1 CH<sub>2</sub> en), 51.96 (1 CH<sub>2</sub> en), 48.52 (2 CH<sub>2</sub> Pyrr), 42.71 (1 C

CH<sub>3</sub>), 42.13 (1C CH<sub>3</sub>), 24.70 (2 C Pyrr). IR (KBr) 1968, 1910, 1900 cm<sup>-1</sup> ( $\nu_{\rm CO}$ ). Anal. Calcd (%) for C<sub>28</sub>H<sub>29</sub>FeN<sub>3</sub>O<sub>3</sub>: C, 65.76; H, 5.72; N, 8.22. Found: C, 65.35; H, 5.76; N, 8.04.

[nBu4N][DCOO]. This compound was synthesized using a modified procedure based on a known synthesis of the protonated compound.<sup>4</sup> Outside of the glovebox with no consideration taken for exposure to moisture or air, 500 mg of [Na][DCOO] was dissolved in 2 mL of D<sub>2</sub>O<sub>2</sub> and concentrated DCl was added until the pH measured ~1 using pH test strips (ca. 0.05 mL). ["Bu<sub>4</sub>N][OH] (7.24 mL; 1.0 M solution in MeOH) was added. Solvent was removed under high vacuum with heating to 100  $^{\circ}$ C. The flask containing the light brown residue was brought into a nitrogen-filled glovebox and dissolved in acetonitrile. This light brown solution was run through a plug of silica gel to give a clear colorless solution. Solvent was removed under high vacuum to give a white solid. <sup>1</sup>H NMR (500 MHz, CD<sub>3</sub>CN)  $\delta$  3.17–3.10 (m, 1H), 1.63 (p, J = 7.9 Hz, 1H), 1.38 (h, J = 7.4 Hz, 1H), 1.03–0.96 (m, 12H). <sup>13</sup>C NMR (126 MHz, CD<sub>3</sub>CN)  $\delta$  58.90, 23.92, 19.90, 13.37. IR (KBr) 1473, ( $\nu_{\rm CO}$ ). Anal. Calcd (%) for C<sub>17</sub>H<sub>36</sub>DN<sub>1</sub>O<sub>2</sub>·0.5H<sub>2</sub>O: C, 68.63; H, 13.21; N, 4.71. Found: C, 68.43; H, 12.97; N, 4.92. Although all precautions were taken to dry the product completely, repeated analyses on independently prepared batches consistently show that it retains 0.5 H<sub>2</sub>O before combustion analysis.

(1-(Cp<sup>N2</sup>)Fe)<sub>2</sub> (4). In a glovebox, F (15 mg, 22.9  $\mu$ mol) was dissolved in acetonitrile, along with [ $^{\rm n}$ Bu<sub>4</sub>N][HCOO] (6.6 mg, 22.9  $\mu$ mol) in a 25 mL Schlenk flask with a Teflon screw valve containing a Teflon-coated stir bar. The flask was heated to 45 °C for 5 days, during which time a black crystalline solid was collected. This material was isolated by filtration, and were suitable crystals for single crystal X-ray diffraction were obtained (5.3 mg, 6.4  $\mu$ mol, 55%). IR (KBr) 1921, 1730 cm<sup>-1</sup> ( $\nu$ CO). Poor solubility prevented solution-phase characterization.

**[Cp**<sup>N3</sup>][B(C<sub>6</sub>F<sub>5</sub>)<sub>4</sub>]. Equimolar amounts of  $[K][B(C_6F_5)_4]$  and  $[Cp^{N3}][BF_4]$  were dissolved in a minimum amount of diethyl ether, giving a white precipitate suspended in a blue solution. This suspension was filtered with a PTFE syringe filter giving a blue solution, which was layered with pentane and stored at -30 °C in a glovebox freezer. Overnight a viscus blue oil formed on the bottom of the vial, and after several weeks at -30 °C, this oil crystallized, giving X-ray-quality crystals (Figure S12). This product was not characterized any further.

**Equilibrium Hydricity Measurement Attempts with BIM** and BIMH. In a nitrogen-filled glovebox, to a J. Young NMR tube were added **2** (10 mg, 19.6  $\mu$ mol) and [Me<sub>5</sub>BzIm][B(C<sub>6</sub>F<sub>5</sub>)<sub>4</sub>] (17 mg, 19.6  $\mu$ mol) in 0.5 mL of acetonitrile- $d_3$  and heated to 45 °C. the reaction was monitored by <sup>1</sup>H NMR for several weeks, and no change occurred. Similar experiments were performed using **1** and [BIM]-[B(C<sub>6</sub>F<sub>5</sub>)<sub>4</sub>], and the same outcome was observed.

Computational Details. Geometries were optimized in the Turbomole<sup>41</sup> v.7.5.1 program package on the efficient r<sup>2</sup>SCAN-3c<sup>32</sup> level of theory with the implicit COSMO<sup>31</sup> solvation model for acetonitrile and tetrahydrofuran (with  $\varepsilon$  = 35.688 for MeCN and  $\varepsilon$  = 7.58 for THF). The m4 integration grid was employed with the radsize increased to 15. With this level of theory, initial guesses for the transition states were obtained with the DE-GSM<sup>42,43</sup> method and then optimized in Turbomole. Single-point energy calculations  $(\Delta E)$ were conducted in Orca<sup>44</sup> v. 5.0.4 with the  $\omega$ B97X-V<sup>28</sup> functional employing the large def2-QZVPP basis set.<sup>29</sup> This method was selected because of its robust performance that has been extensively benchmarked. Thermostatistical corrections ( $\Delta G_{mRRHO}$ ) were obtained with the modified RRHO<sup>16</sup> scheme with T = 318.15 K for the reactions with  $[HCOO]^-$  in MeCN and with T = 298.15 K for all other reactions. Solvation free energies were obtained  $(\delta \Delta G_{\rm solv})^{11}$ with the implicit solvation model COSMO-RS (DFT; COSMOtherm Version C3.0, release 16.01, 2016 parametrization, parameter file: BP TZVP C30 1601.ctd; default Gsolv option) with parametrizations for THF and MeCN.

#### ASSOCIATED CONTENT

# Supporting Information

The Supporting Information is available free of charge at https://pubs.acs.org/doi/10.1021/acs.organomet.4c00137.

NMR spectra, kinetics plots, electrochemistry, additional computational data (PDF)

Computed Cartesian coordinates (ZIP)

#### **Accession Codes**

CCDC 2346231–2346233 contain the supplementary crystallographic data for this paper. These data can be obtained free of charge via <a href="www.ccdc.cam.ac.uk/data\_request/cif">www.ccdc.cam.ac.uk/data\_request/cif</a>, or by emailing <a href="data\_request@ccdc.cam.ac.uk">data\_request/cif</a>, or by contacting The Cambridge Crystallographic Data Centre, 12 Union Road, Cambridge CB2 1EZ, UK; fax: +44 1223 336033.

## AUTHOR INFORMATION

#### **Corresponding Authors**

Andreas Hansen – Mulliken Center for Theoretical Chemistry, Clausius-Institut für Physikalische und Theoretische Chemie, Rheinische Friedrich-Wilhelms Universität Bonn, Bonn 53115, Germany; orcid.org/0000-0003-1659-8206; Email: hansen@thch.uni-bonn.de

Demyan E. Prokopchuk — Department of Chemistry, Rutgers University—Newark, Newark, New Jersey 07102, United States; orcid.org/0000-0002-6352-3509; Email: demyan.prokopchuk@rutgers.edu

#### Authors

Andrew I. VanderWeide — Department of Chemistry, Rutgers University—Newark, Newark, New Jersey 07102, United States

Hagen Neugebauer – Max-Planck-Institut für Kohlenforschung, Mülheim an der Ruhr 45470, Germany; Mulliken Center for Theoretical Chemistry, Clausius-Institut für Physikalische und Theoretische Chemie, Rheinische Friedrich-Wilhelms Universität Bonn, Bonn 53115, Germany; orcid.org/0000-0003-1309-0503

Bhumika Goel – Department of Chemistry, Rutgers University—Newark, Newark, New Jersey 07102, United States

David S. Tresp — Department of Chemistry, Rutgers University—Newark, Newark, New Jersey 07102, United States; © orcid.org/0000-0003-4743-6269

Deuris Pena – Department of Chemistry, Rutgers University—Newark, Newark, New Jersey 07102, United States

Stefan Grimme – Mulliken Center for Theoretical Chemistry, Clausius-Institut für Physikalische und Theoretische Chemie, Rheinische Friedrich-Wilhelms Universität Bonn, Bonn 53115, Germany; orcid.org/0000-0002-5844-4371

Complete contact information is available at: https://pubs.acs.org/10.1021/acs.organomet.4c00137

# **Author Contributions**

 $^{\parallel} A.I.V.d.W.$  and H.N.: These authors contributed equally.

#### Notes

The authors declare no competing financial interest.

#### ACKNOWLEDGMENTS

D.E.P. thanks the National Science Foundation (NSF) for support under Grant 2055097, and S.G. thanks the Deutsche

Forschungsgemeinschaft (DFG) under Grant 1927/16-1. X-ray structural solutions were partly supported by the NSF under Grant 2018753. D.E.P. and D.P. gratefully acknowledge financial support from the Rutgers—Newark Summer Undergraduate Research Program. S.G. and H.N. gratefully acknowledge financial support from the Max Planck Society through the Max Planck fellow program.

#### REFERENCES

- (1) Shapiro, P. J. The evolution of the ansa-bridge and its effect on the scope of metallocene chemistry. *Coord. Chem. Rev.* **2002**, 231 (1), 67–81.
- (2) Enders, M.; Baker, W. R. Synthesis of Aryl- and Heteroaryl-Substituted Cyclopentadienes and Indenes and their Use in Transition Metal Chemistry. *Curr. Org. Chem.* **2006**, *10* (9), 937–953
- (3) Chirik, P. J. Group 4 Transition Metal Sandwich Complexes: Still Fresh after Almost 60 Years. *Organometallics* **2010**, 29 (7), 1500–1517.
- (4) Field, L. D.; Lindall, C. M.; Masters, A. F.; Clentsmith, G. K. B. Penta-arylcyclopentadienyl complexes. *Coord. Chem. Rev.* **2011**, 255 (15), 1733–1790.
- (5) Mas-Roselló, J.; Herraiz, A. G.; Audic, B.; Laverny, A.; Cramer, N. Chiral Cyclopentadienyl Ligands: Design, Syntheses, and Applications in Asymmetric Catalysis. *Angew. Chem., Int. Ed.* **2021**, 60 (24), 13198–13224.
- (6) VanderWeide, A.; Prokopchuk, D. E. Cyclopentadienyl ring activation in organometallic chemistry and catalysis. *Nat. Rev. Chem.* **2023**, *7* (8), 561–572.
- (7) Green, M. L. H.; Pratt, L.; Wilkinson, G. 760. A new type of transition metal—cyclopentadiene compound. *J. Chem. Soc.* **1959**, *0*, 3753—3767.
- (8) Davison, A.; Green, M. L. H.; Wilkinson, G. 620.  $\pi$ -Cyclopentadienyl- and cyclopentadiene-iron carbonyl complexes. *Journal of the Chemical Society (Resumed)* **1961**, 0, 3172–3177.
- (9) Churchill, M.; Mason, R. The crystal and molecular structure of  $\pi$ -cyclopentadienyl 1-phenylcyclopentadiene cobalt. *Philos. Trans. R. Soc. London, Ser. A* **1964**, 279 (1377), 191–209.
- (10) Lehmkuhl, H.; Nehl, H. F. Über (cyclopentadienyl) organylcobalt-komplexe. Chem. Ber. 1984, 117 (12), 3443-3456.
- (11) Davies, S. G.; Green, M. L. H.; Mingos, D. M. P. Nucleophilic addition to organotransition metal cations containing unsaturated hydrocarbon ligands: A survey and interpretation. *Tetrahedron* 1978, 34 (20), 3047–3077.
- (12) Fischer, E. O.; Herberich, G. E. Über aromatenkomplexe von metallen, XLIV. Über die reaktivität des di-cyclopentadienyl-kobalt (III)-kations. *Chem. Ber.* **1961**, *94* (6), 1517–1523.
- (13) Lapinte, C.; Catheline, D.; Astruc, D. Sodium borohydride reduction of carbon monoxide in the cationic iron carbonyl complexes  $[C_5Me_5Fe(CO)_2L]^+$   $PF_6^-$  (L = CO or phosphine). *Organometallics* **1988**, 7 (8), 1683–1691.
- (14) Wiedner, E. S.; Chambers, M. B.; Pitman, C. L.; Bullock, R. M.; Miller, A. J. M.; Appel, A. M. Thermodynamic Hydricity of Transition Metal Hydrides. *Chem. Rev.* **2016**, *116* (15), 8655–8692.
- (15) Pitman, C.; Finster, O.; Miller, A. Cyclopentadiene-mediated hydride transfer from rhodium complexes. *Chem. Commun.* **2016**, 52 (58), 9105–9108.
- (16) Hamon, P.; Hamon, J.-R.; Lapinte, C. Isolation and characterization of a cationic 19-electron iron(III) hydride complex; electron transfer induced hydride migration by carbon monoxide at an iron(III) centre. *J. Chem. Soc., Chem. Commun.* **1992**, 1602–1603.
- (17) Schild, D. J.; Drover, M. W.; Oyala, P. H.; Peters, J. C. Generating Potent C-H PCET Donors: Ligand-Induced Fe-to-Ring Proton Migration from a Cp\*Fe<sup>III</sup>-H Complex Demonstrates a Promising Strategy. *J. Am. Chem. Soc.* **2020**, *142* (44), 18963–18970.
- (18) Chalkley, M. J.; Oyala, P. H.; Peters, J. C. Cp\* Noninnocence Leads to a Remarkably Weak C-H Bond via Metallocene Protonation. *J. Am. Chem. Soc.* **2019**, *141* (11), 4721–4729.

- (19) Sánchez, P.; Goel, B.; Neugebauer, H.; Lalancette, R. A.; Grimme, S.; Hansen, A.; Prokopchuk, D. E. Ligand Protonation at Carbon, not Nitrogen, during H<sub>2</sub> Production with Amine-Rich Iron Electrocatalysts. *Inorg. Chem.* **2021**, *60* (22), 17407–17413.
- (20) Goel, B.; Neugebauer, H.; VanderWeide, A. I.; Sánchez, P.; Lalancette, R. A.; Grimme, S.; Hansen, A.; Prokopchuk, D. E. Essential Roles of Cp Ring Activation and Coordinated Solvent During Electrocatalytic  $H_2$  Production with  $Fe(Cp^{N3})$  Complexes. ACS Catal. 2023, 13, 13650–13662.
- (21) DuBois, D. L.; Berning, D. E. Hydricity of transition-metal hydrides and its role in CO<sub>2</sub> reduction. *Appl. Organomet. Chem.* **2000**, 14 (12), 860–862.
- (22) Miller, A. J. M.; Labinger, J. A.; Bercaw, J. E. Trialkylborane-Assisted CO<sub>2</sub> Reduction by Late Transition Metal Hydrides. *Organometallics* **2011**, *30* (16), 4308–4314.
- (23) Allen, F. H.; Kennard, O.; Watson, D. G.; Brammer, L.; Orpen, A. G.; Taylor, R. Tables of bond lengths determined by X-ray and neutron diffraction. Part 1. Bond lengths in organic compounds. *J. Chem. Soc., Perkin Trans.* 1987, 12, S1–S19.
- (24) Orpen, A. G.; Brammer, L.; Allen, F. H.; Kennard, O.; Watson, D. G.; Taylor, R. Appendix A: Typical Interatomic Distances in Organic Compounds and Organometallic Compounds and Coordination Complexes of the d- and f-block metals. *Structure Correlation* 1994, 752–858.
- (25) Ilic, S.; Alherz, A.; Musgrave, C. B.; Glusac, K. D. Thermodynamic and kinetic hydricities of metal-free hydrides. *Chem. Soc. Rev.* **2018**, 47, 2809–2836.
- (26) Ilic, S.; Pandey Kadel, U.; Basdogan, Y.; Keith, J. A.; Glusac, K. D. Thermodynamic Hydricities of Biomimetic Organic Hydride Donors. J. Am. Chem. Soc. 2018, 140 (13), 4569–4579.
- (27) Lim, C.-H.; Ilic, S.; Alherz, A.; Worrell, B. T.; Bacon, S. S.; Hynes, J. T.; Glusac, K. D.; Musgrave, C. B. Benzimidazoles as Metal-Free and Recyclable Hydrides for CO<sub>2</sub> Reduction to Formate. *J. Am. Chem. Soc.* **2019**, *141* (1), 272–280.
- (28) Mardirossian, N.; Head-Gordon, M.  $\omega$ B97X-V: A 10-parameter, range-separated hybrid, generalized gradient approximation density functional with nonlocal correlation, designed by a survival-of-the-fittest strategy. *Phys. Chem. Chem. Phys.* **2014**, *16*, 9904–9924.
- (29) Weigend, F.; Ahlrichs, R. Balanced basis sets of split valence, triple zeta valence and quadruple zeta valence quality for H to Rn: Design and assessment of accuracy. *Phys. Chem. Chem. Phys.* **2005**, 7 (18), 3297–3305.
- (30) Klamt, A. Conductor-like Screening Model for Real Solvents: A New Approach to the Quantitative Calculation of Solvation Phenomena. *J. Phys. Chem.* **1995**, *99* (7), 2224–2235.
- (31) Klamt, A.; Jonas, V.; Bürger, T.; Lohrenz, J. C. W. Refinement and Parametrization of COSMO-RS. *J. Phys. Chem. A* **1998**, *102* (26), 5074–5085.
- (32) Grimme, S.; Hansen, A.; Ehlert, S.; Mewes, J.-M. r<sup>2</sup>SCAN-3c: A "Swiss army knife" composite electronic-structure method. *J. Chem. Phys.* **2021**, *154* (6), No. 064103.
- (33) Klamt, A.; Schüürmann, G. COSMO: a new approach to dielectric screening in solvents with explicit expressions for the screening energy and its gradient. *J. Chem. Soc., Perkin. Trans.* **1993**, *5*, 799–805.
- (34) Grimme, S.; Hansen, A. A Practicable Real-Space Measure and Visualization of Static Electron-Correlation Effects. *Angew. Chem., Int. Ed.* **2015**, *54* (42), 12308–12313.
- (35) Robinson, W. E.; Bassegoda, A.; Blaza, J. N.; Reisner, E.; Hirst, J. Understanding How the Rate of C-H Bond Cleavage Affects Formate Oxidation Catalysis by a Mo-Dependent Formate Dehydrogenase. *J. Am. Chem. Soc.* **2020**, *142* (28), 12226–12236.
- (36) Williams, D. B. G.; Lawton, M. Drying of Organic Solvents: Quantitative Evaluation of the Efficiency of Several Desiccants. *J. Org. Chem.* **2010**, *75* (24), 8351–8354.
- (37) Motokura, K.; Nakagawa, C.; Pramudita, R. A.; Manaka, Y. Formate-Catalyzed Selective Reduction of Carbon Dioxide to

Formate Products Using Hydrosilanes. ACS Sustainable Chem. Eng. 2019, 7 (13), 11056–11061.

- (38) Han Lee, I.-S.; Kiu Lee, C. NMR Studies of 2-Aryl Derivitives of Benzamidazole, Benzamidazolium Ion, and Benximidazoline. *Heterocycles* **2009**, *78*, 425–433.
- (39) Claisen, L.; Ewan, T. Ueber die Einwirkung des Oxaläthers auf Dibenzylketon. *Justus Liebigs Ann. Chem.* **1895**, 284 (3), 245–299.
- (40) Lator, A.; Gaillard, S.; Poater, A.; Renaud, J.-L. Well-Defined Phosphine-Free Iron-Catalyzed N-Ethylation and N-Methylation of Amines with Ethanol and Methanol. *Org. Lett.* **2018**, *20* (19), 5985–5990
- (41) TURBOMOLE V7.5. 2020, a Development of University of Karlsruhe and Forschungszentrum Karlsruhe GmbH, 1989–2007; TURBOMOLE GmbH, since 2007; http://www.turbomole.org.
- (42) Zimmerman, P. Reliable Transition State Searches Integrated with the Growing String Method. *J. Chem. Theory Comput.* **2013**, 9 (7), 3043–3050.
- (43) Zimmerman, P. M. Growing string method with interpolation and optimization in internal coordinates: Method and examples. *J. Chem. Phys.* **2013**, *138* (18), No. 184102.
- (44) Neese, F. Software update: The ORCA program system—Version 5.0. WIREs Comput. Mol. Sci. 2022, 12 (5), e1606.
- (45) Bursch, M.; Mewes, J.-M.; Hansen, A.; Grimme, S. Best-Practice DFT Protocols for Basic Molecular Computational Chemistry. *Angew. Chem., Int. Ed.* **2022**, *61* (42), No. e202205735.